The Plant Cell, Vol. 26: 1698–1711, April 2014, www.plantcell.org

Plasma Membranes Are Subcompartmentalized into a Plethora of Coexisting and Diverse Microdomains in *Arabidopsis* and *Nicotiana benthamiana*[C][W]

Iris K. Jarsch,[a] Sebastian S.A. Konrad,[a] Thomas F. Stratil,[a] Susan L. Urbanus,[a] Witold Szymanski,[b] Pascal Braun,[c] Karl-Heinz Braun,[a] and Thomas Ott[a,1]

[a] Ludwig-Maximilians-University of Munich, Faculty of Biology, Institute of Genetics, 82152 Martinsried, Germany
[b] Max-Planck-Institute of Molecular Plant Physiology, 14476 Potsdam-Golm, Germany
[c] Department of Plant Systems Biology, Center for Life and Food Sciences Weihenstephan, Technische Universität München, 85354 Freising-Weihenstephan, Germany

Eukaryotic plasma membranes are highly compartmentalized structures. So far, only a few individual proteins that function in a wide range of cellular processes have been shown to segregate into microdomains. However, the biological roles of most microdomain-associated proteins are unknown. Here, we investigated the heterogeneity of distinct microdomains and the complexity of their coexistence. This diversity was determined in living cells of intact multicellular tissues using 20 different marker proteins from *Arabidopsis thaliana*, mostly belonging to the Remorin protein family. These proteins associate with microdomains at the cytosolic leaflet of the plasma membrane. We characterized these membrane domains and determined their lateral dynamics by extensive quantitative image analysis. Systematic colocalization experiments with an extended subset of marker proteins tested in 45 different combinations revealed the coexistence of highly distinct membrane domains on individual cell surfaces. These data provide valuable tools to study the lateral segregation of membrane proteins and their biological functions in living plant cells. They also demonstrate that widely used biochemical approaches such as detergent-resistant membranes cannot resolve this biological complexity of membrane compartmentalization in vivo.

INTRODUCTION

Plasma membranes (PMs) are highly organized structures that are partitioned in different types of membrane domains (reviewed in Kusumi et al., 2012; Malinsky et al., 2013). Prominent examples are the basolateral membrane of root epidermal cells that is labeled by the polarly localized PIN-FORMED auxin efflux carrier PIN2 (Müller et al., 1998), the Casparian strip that is targeted by CASP proteins (Roppolo et al., 2011), and focal accumulation of the MILDEW RESISTANCE LOCUS O protein at perihaustorial membranes during plant–microbe interactions (Bhat et al., 2005). However, most of these higher order membrane regions are further subdivided. The largest unit, recently defined as the "membrane compartment," is between 40 and 300 nm in diameter and mainly determined by cortical cytoskeleton elements that restrict the lateral diffusion of membrane-associated proteins (Kusumi et al., 2012). Similar structures have also been described in other eukaryotic cells such as *Saccharomyces cerevisiae* (yeast) (Malinsky et al., 2010; Spira et al., 2012). "Membrane rafts" can be found within these compartments. They are substantially smaller (2 to 20 nm) and characterized by their enrichment in sterols and sphingolipids (Boutté and Grebe, 2009). The molecular interactions between these membrane components have been shown to lead to a spatial phase transition toward a more liquid-ordered state in model membranes. Targeting of proteins to membrane rafts is often achieved by posttranslational modifications such as the addition of glycosylphosphatidylinositol and *S*-acyl (palmitoyl) moieties (Levental et al., 2010a, 2010b) or by electrostatic interactions (van den Bogaart et al., 2011). Physical interaction between raft-localized proteins and/or molecular scaffolds can lead to the clustering of nanoscale domains into larger units, recently defined as "raft platforms," or membrane microdomains (Lingwood and Simons, 2010). These domains can almost reach micrometer ranges and are believed to harbor defined sets of preassembled signaling protein complexes, including components of the innate immune system. In plants, unfortunately and misleadingly, for a long time membrane domains have been equalized with detergent-resistant membranes (DRMs). DRMs derive from a biochemical extraction with nonionic detergents such as Triton X-100 in the cold. However, the specificity of DRMs has been widely questioned over the years, as sterols have the biophysical tendency to aggregate into large sheets that do not reflect individual microdomains in vivo (Zurzolo et al., 2003; Tanner et al., 2011; Malinsky et al., 2013).

A number of recent cell biological approaches revealed membrane-associated proteins such as Flotillins and Remorins to label distinct microdomains in living cells (Raffaele et al., 2009; Haney and Long, 2010; Lefebvre et al., 2010; Haney et al.,

[1] Address correspondence to thomas.ott@bio.lmu.de.
The author responsible for distribution of materials integral to the findings presented in this article in accordance with the policy described in the Instructions for Authors (www.plantcell.org) is: Thomas Ott (thomas.ott@bio.lmu.de).
[C] Some figures in this article are displayed in color online but in black and white in the print edition.
[W] Online version contains Web-only data.
www.plantcell.org/cgi/doi/10.1105/tpc.114.124446

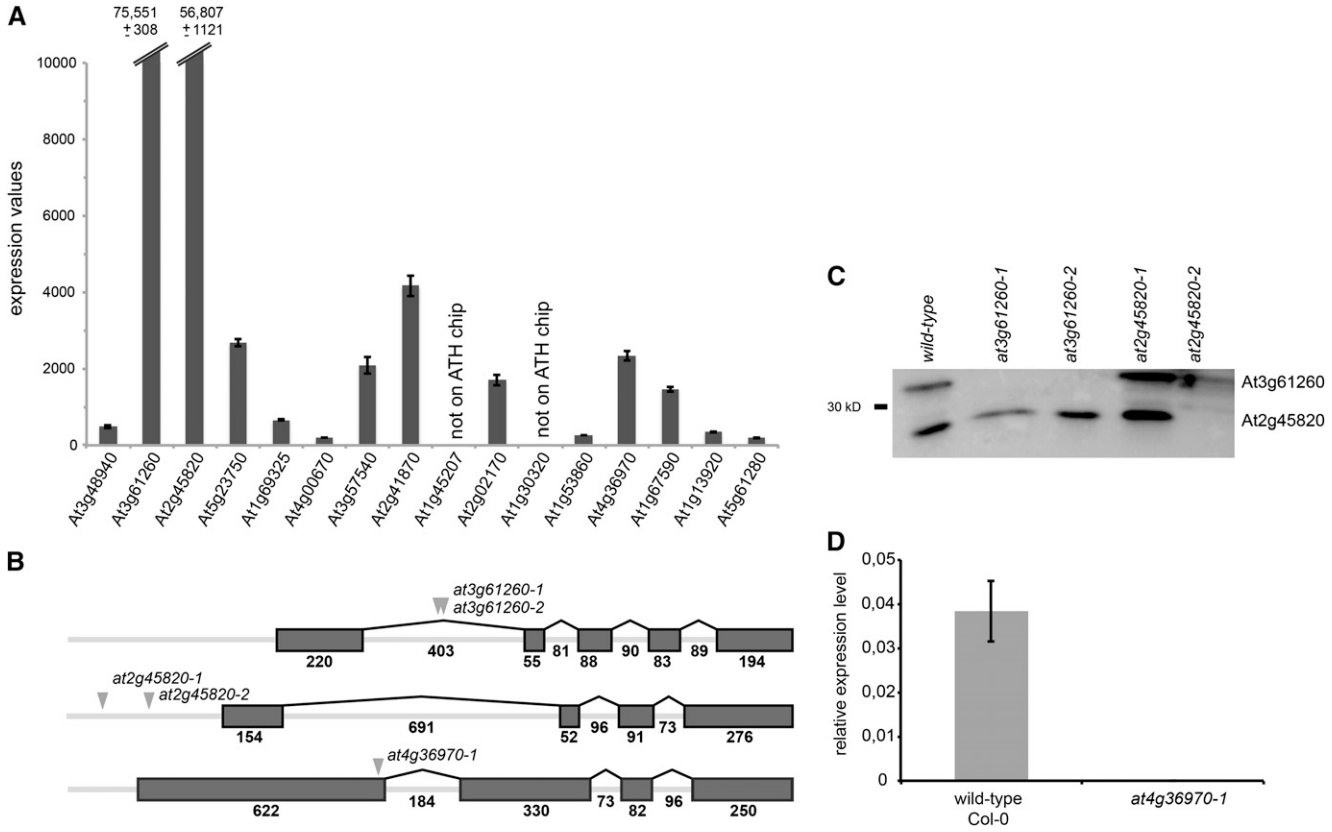

Figure 1. Remorin Expression Patterns and Identification of Homozygous Knockout Mutants.

(A) Data were obtained from the publicly available Genevestigator database (https://www.genevestigator.com/gv/plant.jsp). Error bars represent SE of three independent biological experiments. ATH chip, *Arabidopsis* Affymetrix chip.

(B) Schematic representation of the Remorin genes *At3g61260*, *At2g45820*, and *At4g36970*. Triangles indicate the T-DNA insertion sites, and gray boxes indicate the exons of the genes.

(C) Protein gel blot analysis of different *at3g61260* and *at2g45820* mutants confirmed the absence of the respective proteins in three of these lines. An α-REM antibody that was originally raised against the potato REM1.3 recognizes the two most closely related proteins in *Arabidopsis*.

(D) Quantitative real-time PCR analysis of three independent biological replicates confirmed the lack of transcript in the *at4g36970-1* mutant line. Error bars represent SE. Col-0, Columbia-0.

2011; Li et al., 2012; Demir et al., 2013). As in mammalian cells, Flotillins form a small gene family with only three members (*At5g25250*, *At5g25260*, and *At5g64870*) in *Arabidopsis thaliana*, while the plant-specific Remorin family comprises 16 genes (Raffaele et al., 2007). All Remorin proteins contain a canonical C-terminal region (Raffaele et al., 2007), and the majority of them contain an intrinsically disordered N-terminal segment that varies greatly in length and sequence but harbors almost all in vivo phosphorylation sites (Marín and Ott, 2012; Marín et al., 2012). Localization of single Remorins to membrane domains has been shown for ectopically expressed REM1.3 from potato (*Solanum tuberosum*), for an endogenous Remorin from tomato (*Solanum lycopersicum*; Raffaele et al., 2009), as well for the closely related protein from *Arabidopsis* (REM1.3/At2g45820) (Demir et al., 2013). Furthermore, immunolocalization of the legume-specific SYMBIOTIC REMORIN1 (SYMREM1) protein from *Medicago truncatula* revealed domain-localized patterns along infection threads that encapsulate symbiotic bacteria during root nodule symbiosis (Lefebvre et al., 2010). While the potato REM1.3 regulates viral movement (Raffaele et al., 2009), SYMREM1 is required for successful infection by rhizobia and interacts via its predicted coiled-coil domain with receptor-like kinases such as the LYSIN-MOTIF RECEPTOR KINASE3 (LYK3) and the NOD FACTOR RECEPTOR1 (NFR1) (Lefebvre et al., 2010; Tóth et al., 2012). Interestingly, LYK3 also localizes to membrane domains. Upon perception of symbiotic rhizobia by the host plant, LYK3 mobility is laterally arrested, resulting in a colocalization with the domains labeled by the Flotillin protein FLOT4 (Haney et al., 2011). It remains to be shown whether both proteins interact physically in these membrane domains. However, such compartmentalized interactions have been demonstrated by fluorescence lifetime imaging microscopy between a number of proteins: the hypervariable region of a small maize (*Zea mays*) GTPase ROP7 and the CALCIUM-DEPENDENT PROTEIN KINASE1 (CPK1) (Vermeer et al., 2004), for homooligomeric complexes of the brassinosteroid receptor BRASSINOSTEROID INSENSITIVE1 (BRI1), for BRI1 in a heteromeric complex with the SOMATIC EMBRYOGENESIS RECEPTOR KINASE3 (SERK3) (Russinova et al., 2004), as well as for a complex between the AAA ATPase CDC48A and SERK1 (Aker

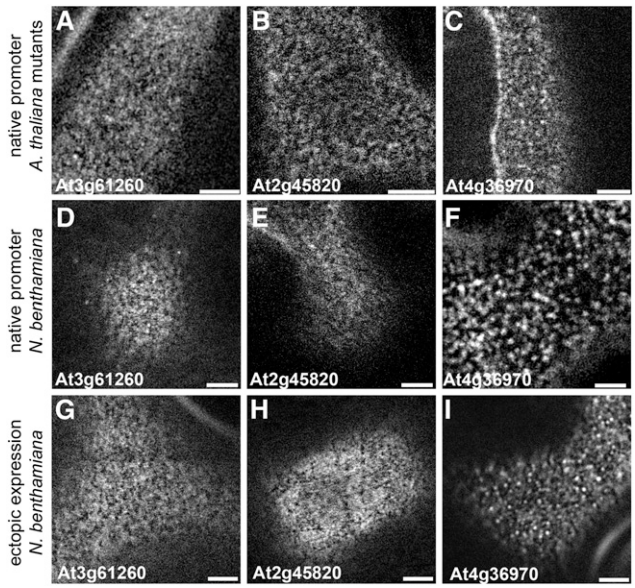

Figure 2. Labeling of Membrane Domains Can Be Consistently Observed in Different Biological Systems.

(A) to **(C)** Homozygous *Arabidopsis* knockout mutants were transformed with the respective fluorophore-tagged Remorins expressed under the control of their endogenous promoters. Bars = 5 µm.
(D) to **(F)** Domain patterning was observed in *N. benthamiana* leaf epidermal cells where the respective genes were expressed under the control of the endogenous *Arabidopsis* promoter. Bars = 5 µm.
(G) to **(I)** Domain patterning was observed in *N. benthamiana* leaf epidermal cells where the respective genes were ectopically expressed under the control of the cauliflower mosaic virus 35S promoter. Bars = 5 µm.

et al., 2007). These data suggest that lateral segregation of proteins into membrane microdomains, either constitutively or in a stimulus-dependent manner, may be an integral determinant for their functionality. These studies ultimately raise the question of how heterogeneous PMs are. In plants, microdomains, especially when being targeted by proteins belonging to the same family, have so far been regarded as one uniform pattern. Here, we show that this concept has to be substantially refined, as single cell membranes in *Arabidopsis* and *Nicotiana benthamiana* are virtually covered with different types of microdomains. These may serve as platforms for interactions between different types of membrane-resident proteins and contribute to their functions.

RESULTS

Identification of Membrane Domain Patterns in Different Experimental Systems

As this study aims to characterize the diversity and dynamics of membrane domains in living plant cells by imaging-based approaches, we first validated our experimental systems carefully. Three Remorin genes (*At3g61260*, *At2g45820*, and *At4g36970*) were chosen based on available expression data. *At3g61260* and *At2g45820* are more than 20-fold higher expressed compared with any other member of this multigene family (Figure 1A) and are the most studied ones. To select a structurally different Remorin (Raffaele et al., 2007), *At4g36970*, which is expressed at intermediate levels, was additionally used for this initial analysis. For these genes, *Arabidopsis* T-DNA insertion lines were obtained from the public stock center and homozygous mutant lines were selected. The respective insertion sites are illustrated in Figure 1B. To test if these lines were knockouts, protein or transcript levels were determined. Using the previously described α-REM antibody (Raffaele et al., 2009), which also recognizes the two most abundant *Arabidopsis* Remorins (At3g61260 and At2g45820), we confirmed that both *at3g61260* mutant lines were null alleles, while the At2g45820 protein was no longer expressed in only one line (*at2g45820-2*) (Figure 1C). Thus, this line was used for further analysis. As no antibody was available for At4g36970, transcript levels of this gene were determined using quantitative real-time PCR. Indeed, no *At4g36970* transcript was detectable in the *at4g36970-1* mutant (Figure 1D). Next, we transformed *at3g61260-2*, *at2g45820-2*, and *at4g36970-1* with constructs expressing the respective genes as N-terminally tagged fusion proteins under the control of their native promoters (e.g., *ProAt3g61260-YFP:At3g61260*). To obtain a detailed view of the membrane domains, confocal laser scanning microscopy (CLSM) was used to image the upper surface plane of rosette leaf epidermal cells of 3- to 4-week-old plants. A diffuse but structured labeling of the PM was observed for the two highly expressed Remorins At3g61260 and At2g45820 (Figures 2A and 2B). By contrast, At4g36970 segregated into more distinct microdomains (Figure 2C). The same results were obtained upon expression of these constructs under the control of their native promoter (Figures 2D to 2F) or the constitutively active cauliflower mosaic virus 35S promoter (Figures 2G to 2I) in *N. benthamiana* leaf epidermal cells.

To further verify these results, the subcellular localization of another weakly expressed Remorin protein (*At5g61280*) was investigated. A *ProAt5g61280-YFP:At5g61280* construct was transiently transformed into leaf epidermal cells of a transgenic *Arabidopsis* line that expresses the bacterial effector AvrPto under the control of a dexamethasone-inducible promoter (*ProDex-AvrPto*) (Hauck et al., 2003). Induction of *AvrPto* expression leads to the degradation of plant immune receptors and thus allows efficient transient transfection of cells by *Agrobacterium tumefaciens* (Tsuda et al., 2012). In *Arabidopsis*, At5g61280 was only weakly expressed but localized to distinct membrane domains (Supplemental Figure 1A).

As the observed patterns for At3g61260 and At2g45820 (Figure 2) did not resemble the results from a recent report where strong overexpression of At2g45820 after ballistic transformation resulted in an accumulation of the protein in large clusters (Demir et al., 2013), we performed total internal reflection microscopy (TIRFM), which allows higher resolution in the *z* axis on our transgenic lines. Indeed, expression of both group 1 Remorins under the control of their endogenous promoters showed the same weakly structured pattern (Supplemental Figure 2) as observed by CLSM. To further verify the robustness of our experimental systems, we studied the localization of the previously reported potato Remorin REM1.3.

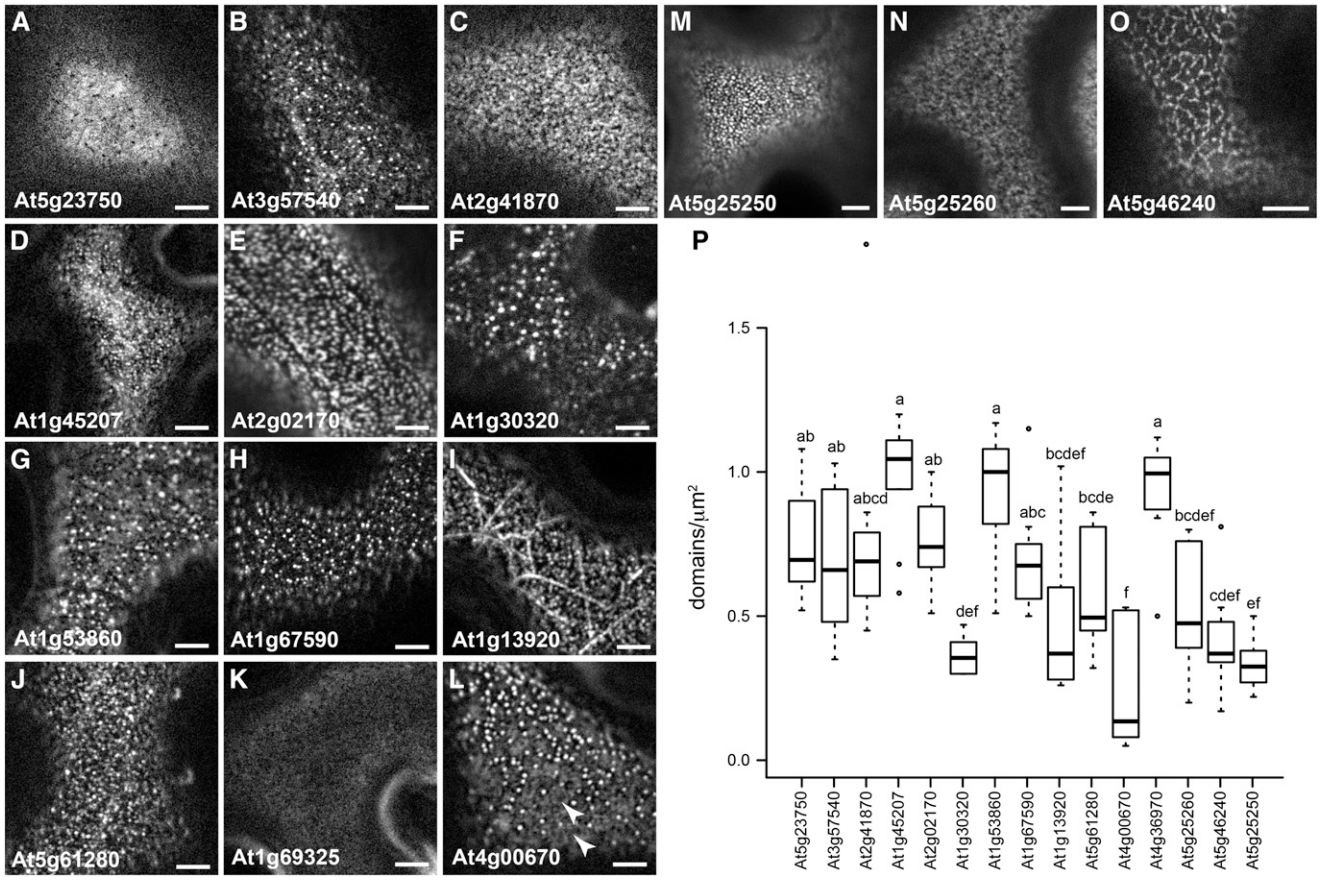

Figure 3. Remorin Proteins, Flotillins, and KAT1 Label a Variety of Distinct Membrane Domains in *N. benthamiana*.

(A) to **(L)** Surface imaging of upper leaf epidermal cell planes expressing 12 different fluorophore-tagged Remorin proteins using CLSM. Bars = 5 µm.
(M) and **(N)** Leaf epidermal cell planes expressing the fluorophore-tagged Flotillin proteins FLOT1A **(M)** and FLOT1B **(N)**. Bars = 5 µm.
(O) Leaf epidermal cell plane expressing the fluorophore-tagged potassium channel KAT1. Bar = 5 µm.
(P) Quantitative image analysis revealed that the average density of membrane domains varied significantly between the different marker proteins. Letters indicate results of a one-way ANOVA followed by Tukey's honestly significant difference test.

Indeed, GFP-REM1.3 also localized to distinct microdomains in *N. benthamiana* leaf epidermal cells (Supplemental Figure 1B).

Similarly, the phylogenetically related SYMREM1 protein was also frequently found to label distinct membrane domains in this system (Supplemental Figure 1C).

Remorin and Flotillin Proteins Label a Large Variety of Membrane Domains

To globally assess the diversity of microdomains, 12 additional Remorins, the two *Arabidopsis* Flotillins FLOT1A (At5g25250) and FLOT1B (At5g25260), and the POTASSIUM CHANNEL IN ARABIDOPSIS THALIANA1 (KAT1) were cloned and ectopically expressed as yellow fluorescent protein (YFP)-tagged fusion proteins in *N. benthamiana* leaf epidermal cells (Figure 3). Imaging of single secant planes revealed PM association of all proteins (Supplemental Figure 3). However, At1g69325, At1g53860, At1g13920, and At5g61280 exhibited partial nuclear and minor cytosolic localization (Supplemental Figures 3D, 3K, 3N, and 3O, arrowheads). To further verify that the observed patterns were not caused by heterologous expression of the proteins, a representative subset (At4g00670, At3g57540, At1g45207, At2g02170, At1g30320, and At1g53860) was expressed in the above-mentioned *ProDex-AvrPto Arabidopsis* lines. All proteins displayed patterns similar to those observed in *N. benthamiana* (Supplemental Figures 1D to 1I).

To describe the patterns in more detail, 10 individual images per construct were subjected to quantitative image analysis. Parameters such as domain size, domain width, mean domain intensity, and circularity (Supplemental Figure 4) as well as domain density (Figure 3P) were determined. It should be noted that even if this analysis is restricted by the resolution limits of CLSM, domains observed in this study were generally larger (Supplemental Figure 4B). As expected, no domains were identified for the rather homogenously distributed proteins At3g61260, At2g45820 (Figure 2), and At1g69325 (Figure 3K). However, At5g23750, which is phylogenetically close to At3g61260 and At2g45820, showed a more structured pattern

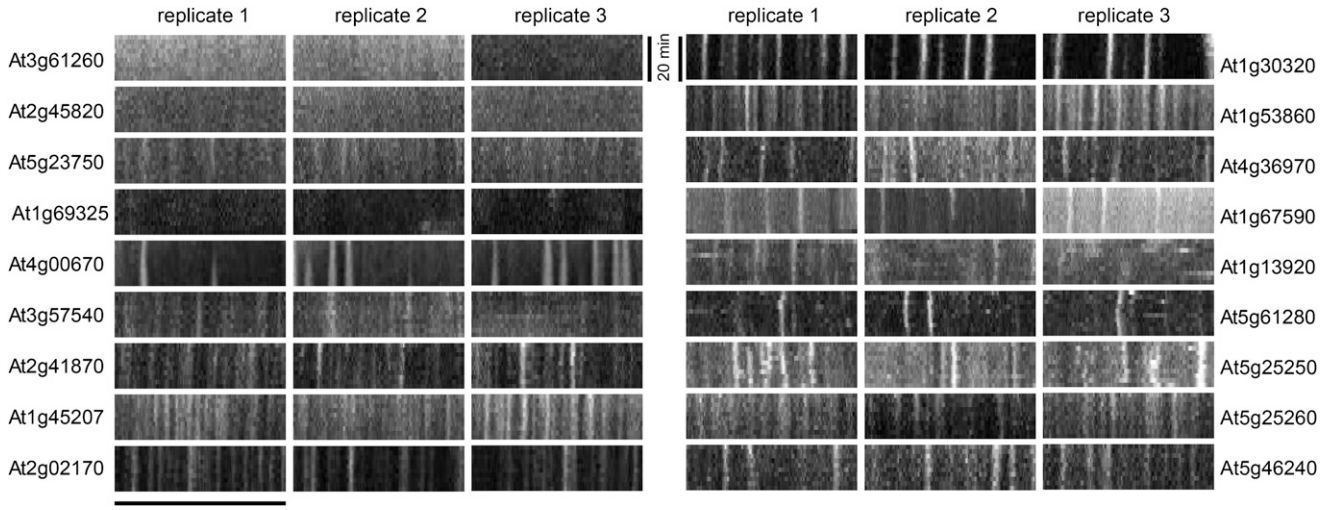

Figure 4. Kymographs Indicate the Lateral Stability of Membrane Domains.

The temporal and lateral mobility of membrane domains was investigated over 20 min in 2-min intervals. Vertical lines in kymographs indicate the lateral stability of most membrane domains. Movement was observed in the case of At1g13290 and partially in the case of At5g61280. The punctate structures appearing at single time points when imaging the Flotillin At5g25250 may represent endosomes. Bars = 20 μm (horizontal) and 20 min (vertical).

(Figure 3A), with an average domain size of ~0.28 μm^2 and an intermediate domain density of 0.75 domains/μm^2 (Figure 3P; Supplemental Figure 4). All other proteins localized to distinct microdomains (Figures 3B to 3J) of different size, shape, and density. While most of the marker proteins labeled membrane domains of ~0.25 μm^2 on average, proteins like At3g57540, At4g36970, At5g61280, and At5g25260 targeted domains that were significantly smaller (Figure 3; Supplemental Figure 4). Two marker proteins, At4g00670 (Figure 3L) and At1g13920 (Figure 3I), showed more distinct patterns. In general, the fluorescence of domains observed for At4g00670 was more intense (Supplemental Figure 4C) and domain density was significantly reduced but varied greatly (Figure 3P) compared with all other marker proteins. Furthermore, this protein labeled a larger homogenously distributed fraction at the PM in addition to distinct membrane domains (Figure 3L; Supplemental Figure 1D, arrowheads). Interestingly, we repeatedly observed that At1g13920 labeled filamentous structures while it additionally localized to more canonical membrane domains in the same cell (Figure 3I). In agreement with published data, the Flotillin proteins At5g25250 (FLOT1A) and At5g25260 (FLOT1B) labeled distinct microdomains (Figures 3M and 3N). FLOT1A-targeted domains varied significantly in size, while FLOT1B domains were relatively small (below 0.2 μm^2) (Figure 3P; Supplemental Figure 4). When using another domain-localized protein, the potassium channel KAT1 (At5g46240), domains appeared stretched and network-like (Figure 3O). These observations are in full agreement with localizations reported for KAT1 earlier (Sutter et al., 2006).

Membrane Microdomains Are Temporally Stable Structures

Next, we asked whether the observed domains represent laterally stable structures. To assess this feature in more detail, we performed time-lapse experiments on all 18 marker proteins. PM surfaces were imaged in 120-s intervals for 20 min, and kymographs were generated. Data obtained from these experiments clearly demonstrated high degrees of lateral stability for most of the observed membrane domains (Figure 4). Since At3g61260, At2g45820, and At1g69325 labeled the membrane more homogenously (Figure 3), the temporal stability of these proteins could not be resolved by this method. Furthermore, a certain degree of lateral movement was observed for At4g36970, At1g13920, and At5g61280. For the latter two proteins, this may reflect the partial cytosolic protein fraction. However, microdomains for these proteins were also temporally stable, as indicated by the vertical lines (Figure 4). In addition, we observed some mobility in At5g25250 (FLOT1A)–expressing cells, which may represent endocytotic vesicles that were described for this protein earlier (Li et al., 2012).

Assessing Lateral Mobility by Fluorescence Recovery after Photobleaching

To characterize the lateral mobility of microdomain marker proteins in more detail, we performed extensive fluorescence recovery after photobleaching (FRAP) analysis on a subset of seven Remorin proteins (Figure 5A). For this, a circular region of interest (ROI) was bleached by high-intensity laser emission for 10 frames (~15 s). Fluorescence recovery on membrane surface areas was assessed over 5 min in 30-s intervals, and data were normalized to a reference ROI of equal size that was placed in close proximity to the bleached one. To compare these data with a cytosolic protein, we expressed soluble YFP in addition. In all samples, fluorescence recovered monoexponentially with coefficient of determination (R^2) > 0.97 (Figure 5A). In general, membrane surfaces labeled by domain marker proteins recovered significantly slower compared with the cytosolic YFP control, with half-times of 24.3 ± 1.4 s (At1g13920 filaments) to

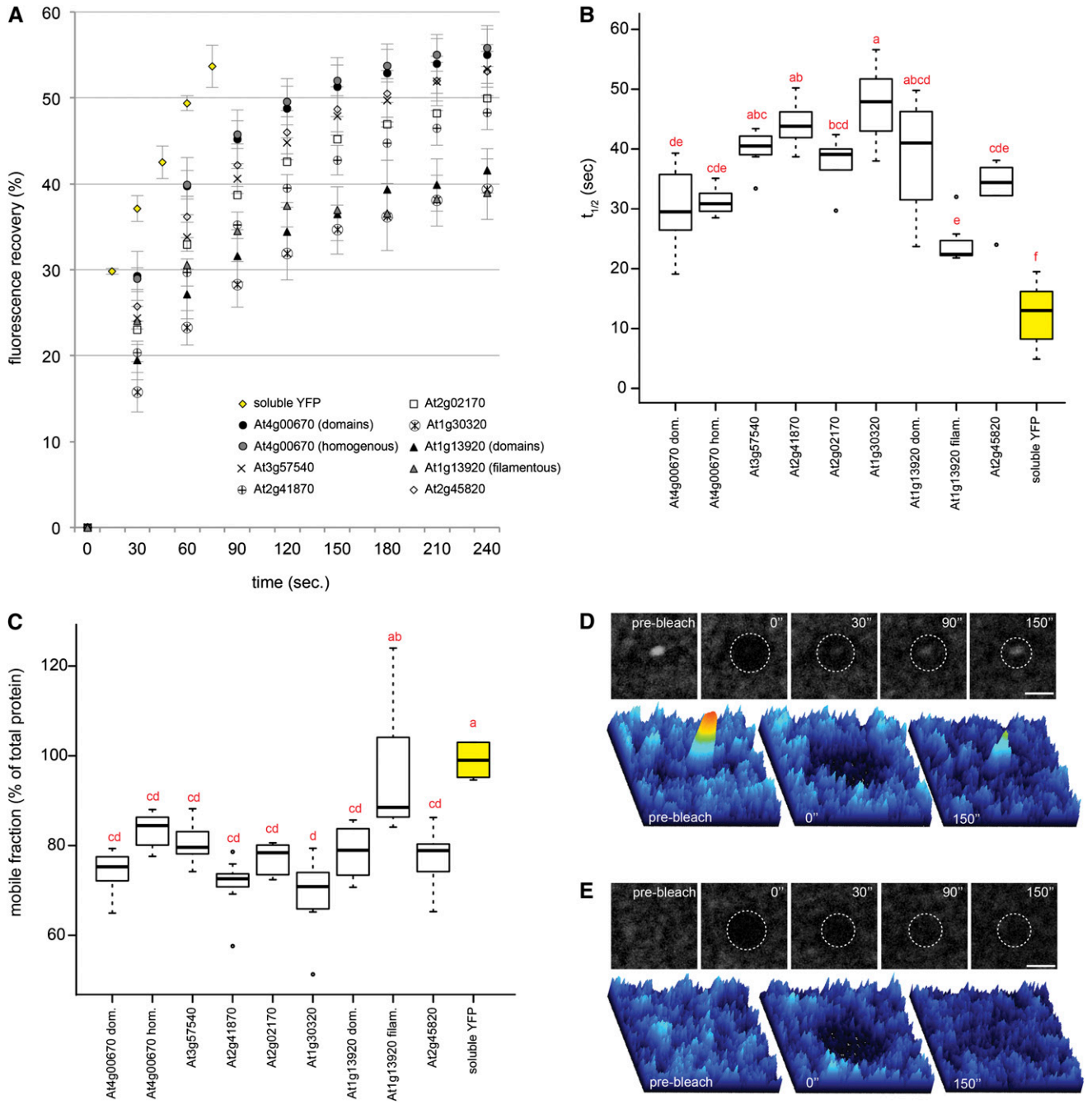

Figure 5. Assessing Protein Mobility by FRAP Analysis.

FRAP was used to investigate the mobility of different marker proteins.

(A) Fluorescence recovery was measured in a minimum of 12 independently bleached ROIs and normalized to nonbleached ROIs in their direct vicinity. Error bars show SE.

(B) and **(C)** Half-times ($t_{1/2}$) **(B)** and mobile fractions **(C)** were calculated for all proteins as described in Methods. Letters indicate results of a one-way ANOVA followed by Tukey's honestly significant difference test. dom., domain-localized protein fraction; hom., homogenously distributed protein fraction; filam., filamentous protein fraction.

(D) Bleaching of individual membrane domains of At4g00670 resulted in recovery at the same position. Panels at top show the images that were used for plotting the corresponding pixel intensities (bottom). Numbers indicate seconds after bleaching. Bar = 2 μm.

(E) Bleaching of the homogenous protein fraction of At4g00670. Fluorescence was centripetally recovered over time. Panels at top show the images that were used for plotting the corresponding pixel intensities (bottom). Numbers indicate seconds after bleaching. Bar = 2 μm.

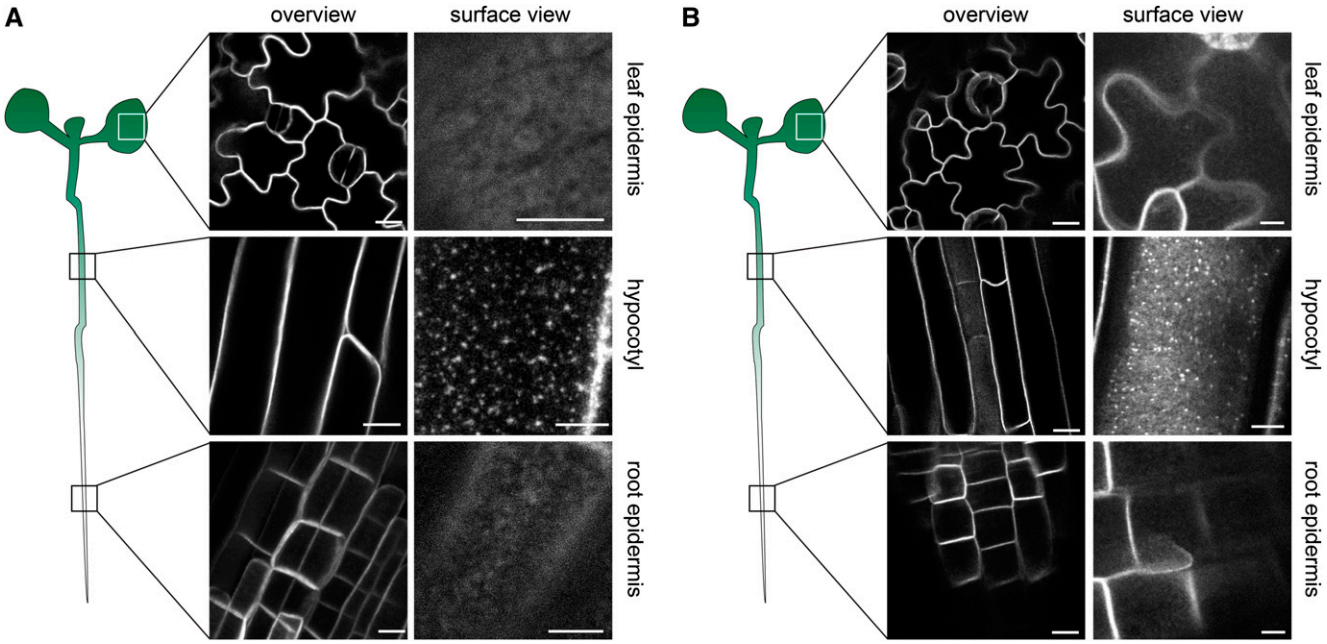

Figure 6. Tissue-Specific Formation of Membrane Domains.

(A) Upper planes of leaf epidermal cells (top panels), elongating hypocotyl cells (middle panels), and root epidermal cells (bottom panels) were imaged in 5-d-old seedlings of transgenic *Arabidopsis at3g61260-1* mutant plants expressing the Remorin protein At3g61260 as an N-terminally tagged YFP fusion protein under the control of its native promoter. Bars = 10 μm (left column) and 5 μm (right column).
(B) Localization studies as in **(A)** but of YFP-At2g45820 expressed in an *at2g45280-2* mutant background under the control of its native promoter. Bars = 10 μm (left column) and 5 μm (right column).
[See online article for color version of this figure.]

47.7 ± 1.9 s (At1g30320) and 12.4 ± 2.6 s, respectively (Figure 5B). However, significant differences were observed between the proteins, with At1g30320 being the most slowly diffusing protein. In the case of At4g00670, no difference in fluorescence recovery between the domain-associated fraction and the homogenously PM-labeling fraction was observed (Figure 5B). Moreover, when bleaching single membrane domains labeled by At4g00670, proteins accumulated in the same position (Figure 5D) while non-domain-labeled PM segments recovered homogenously (Figure 5E). This indicates a physical structure underlying protein accumulation in these distinct positions. Interestingly, At1g13920 again showed a significantly different pattern. While the domain-localized protein fraction overall recovered slowly, the half-time of filament-associated At1g13920 was significantly smaller (Figure 5B). This was also reflected in the mobile fraction, which was significantly increased for filament-associated At1g13920, while no differences were observed between the other Remorin proteins (Figure 5C).

As filament-like structures targeted by At1g13920 were stable over time (Supplemental Figure 5A), we assumed that they do not represent cytosolic strands. To test whether they are dependent on cortical cytoskeleton elements such as microtubules (labeled by MAP4; Supplemental Figure 5B) or actin (labeled by LifeAct; Supplemental Figure 5C), we depolymerized actin and microtubules by the drugs latrunculin B and oryzalin, respectively. While these structures entirely disappeared upon oryzalin treatment and resulted in a predominantly cytosolic localization of At1g13920 (Supplemental Figure 5D), latrunculin B treatment did not alter the At1g13920-labeled filaments (Supplemental Figure 5E). These data indicate that microtubules affect the localization of At1g13920.

Tissue-Specific Labeling of Membrane Microdomains

As described above, At3g61260 and At2g45820 were not targeted to distinct membrane domains in mature rosette leaves in stable transgenic lines where both genes were expressed under the control of their endogenous promoters (Figures 2A and 2B). Thus, we tested whether membrane domains may be labeled in a tissue-specific manner. For this, we imaged different tissues in 3- and 5-d-old seedlings that were grown under sterile conditions. In both cases, we did not observe distinct membrane domains in leaf and root epidermal cells (Figure 6). By contrast, both proteins were occasionally targeted to distinct membrane domains in elongating hypocotyl cells (Figure 6, middle panels). There, they labeled foci in the PM that were similar to those observed for other Remorin proteins. These data indicate that membrane domains are dynamically formed or disintegrated under different environmental conditions or developmental stages.

Coexisting Microdomains Shape Multifaceted PMs

Using a subset of different domain marker proteins, we assessed the coexistence of microdomains on the same cell

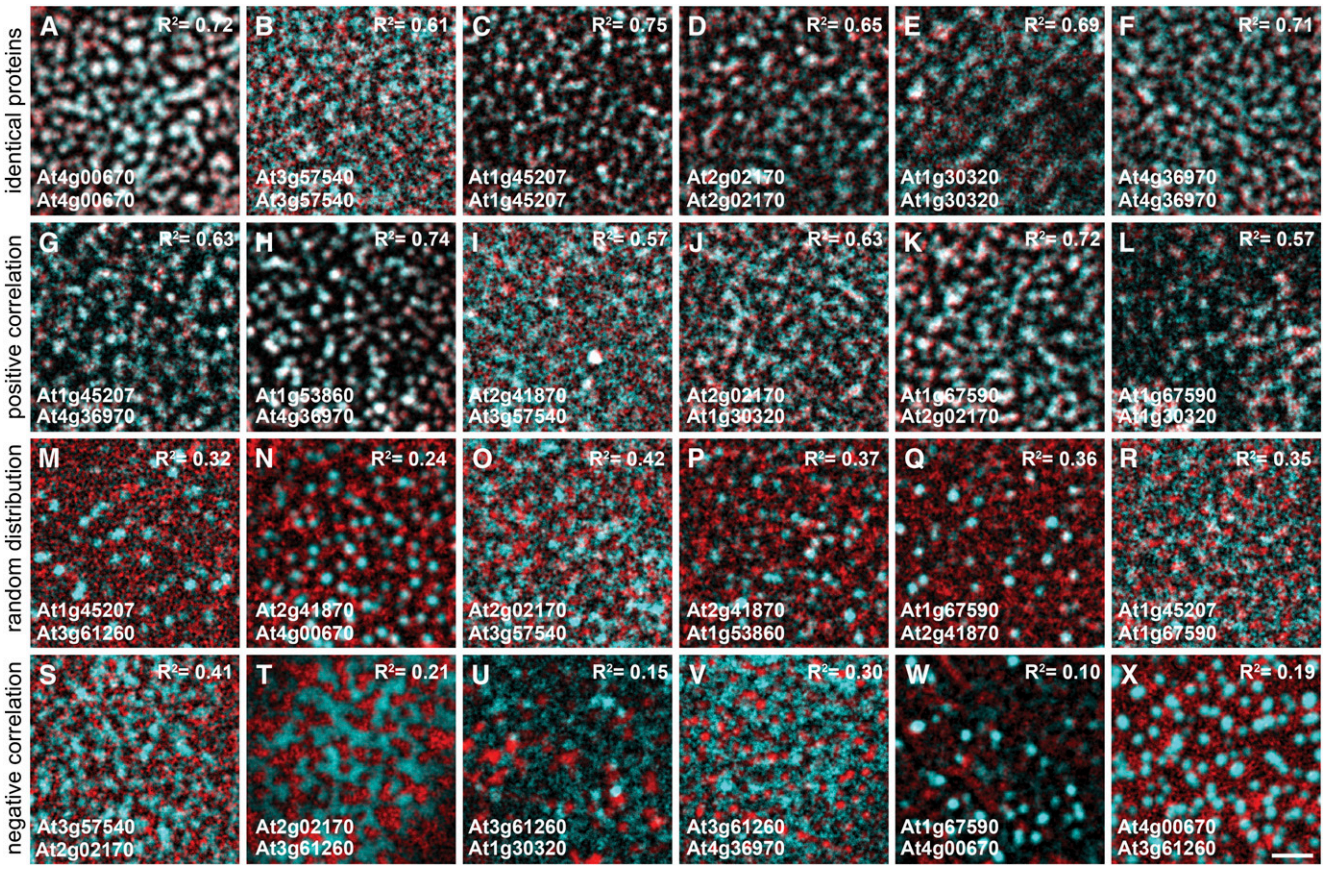

Figure 7. PMs Comprise a Wide Spectrum of Coexisting Microdomains.

(A) to **(F)** Representative images from control experiments where domains were labeled by the same proteins that were tagged with two different fluorophores, CFP (red) and YFP (cyan). R^2 values, which were significantly higher compared with those of the corresponding randomized images, indicate full colocalization of the proteins.

(G) to **(L)** Representative images of protein pairs that showed positive correlation. R^2 values were significantly higher compared with those of the corresponding randomized images. These proteins mutually excluded each other.

(M) to **(R)** Representative images of protein pairs randomly colocalized with each other. R^2 values were not significantly different from those of the corresponding randomized images.

(S) to **(X)** Representative images of protein pairs that showed negative correlation. R^2 values were significantly lower compared with those of the corresponding randomized images. These proteins mutually excluded each other.

Bar in **(X)** = 2 μm for **(A)** to **(X)**.

membrane. An extensive cross-comparison with a total number of 45 colocalization experiments was performed using different domain marker proteins tagged with either cyan fluorescent protein (CFP) or YFP. In all cases, the weakest expressing cells were chosen for image acquisition to minimize possible impacts by overexpression and to resemble the native situation as closely as possible. For each colocalization experiment, an average of 12 single images were subjected to quantitative image analysis. The R^2 (Manders et al., 1993) (Figure 7; Supplemental Table 1) and the standard Pearson correlation coefficient (Manders et al., 1992) (Supplemental Table 1) were calculated for each individual image. To determine the random overlap coefficient, each corresponding channel 2 image (YFP fluorescence) was flipped by 180° and merged with the original image from the CFP channel (Supplemental Figure 6). A Student's *t* test was then applied to determine whether the difference between the two values was significant. Pairs with $R^2 > R^2$ random (positive correlations) were regarded as colocalizing and pairs with $R^2 < R^2$ random (negative correlations) were scored as excluding proteins. Combinations that did not pass the significance level ($P < 0.05$) were designated as randomly colocalized with each other and thus could not be assigned to either of the two categories.

To verify our approach, we first tested nine different pairs, where the same proteins were fused to YFP and CFP. On average, R^2 values of 0.645 were obtained, with the highest value at $R^2 = 0.752$ for At1g45207 (Figure 7C; Supplemental Table 1). These coefficients are fully consistent with the colocalization of microdomain-localized protein pairs previously described for living cells (Spira et al., 2012; Demir et al., 2013). Due to its homogenous distribution, At3g61260 showed the lowest value.

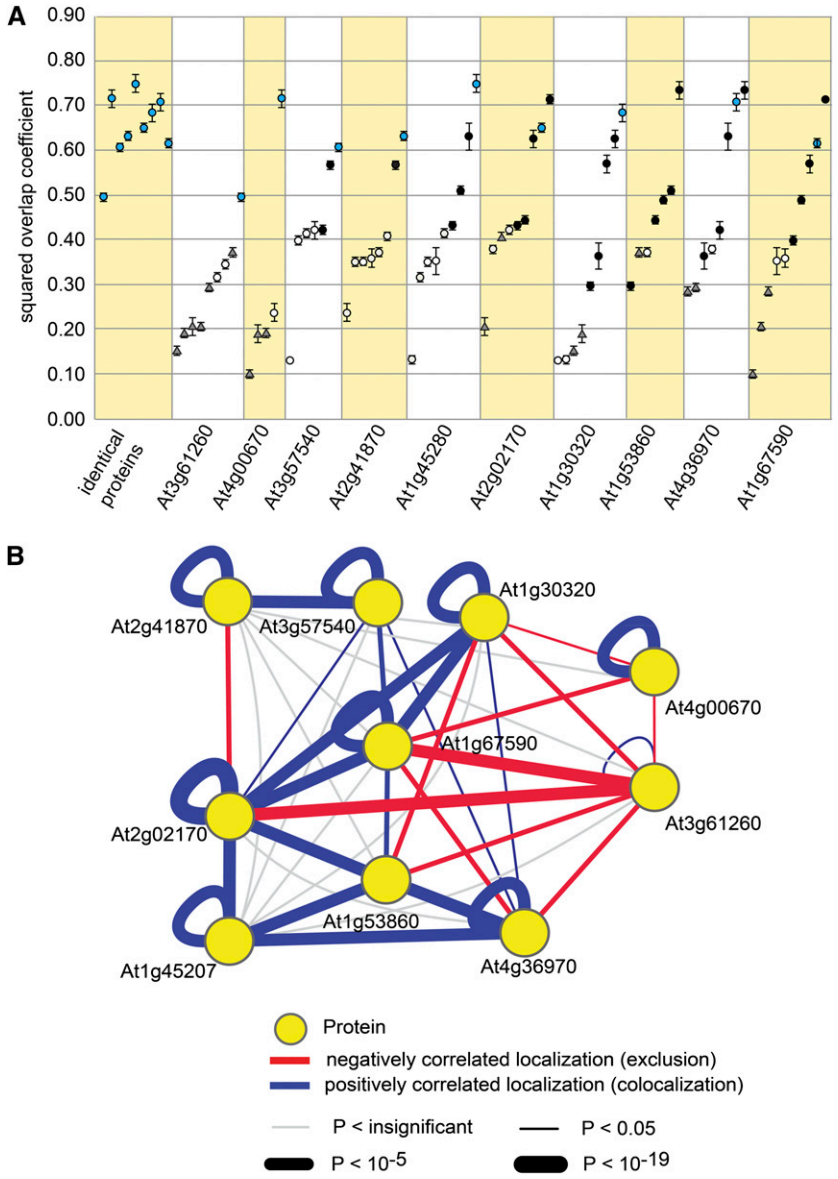

Figure 8. Quantifications and Network Analysis of Membrane Domain Colocalizations.

(A) R^2 values of all tested combinations were plotted in relation to individual proteins. The columns show R^2 values for identical protein pairs (blue circles) that all showed positive correlations. For all other combinations, positive correlations are depicted as black circles, randomly colocalizing combinations as white circles, and pairs with negative correlation as gray triangles. Error bars represent SE.

(B) Network analysis of domain colocalizations revealed that Remorins of subgroup 6 often colocalized, while proteins such as At3g61260 and At4g00670 represent particular membrane domains or compartments.

Testing another 36 different combinations, we identified 14 colocalizing pairs and 12 combinations that strictly excluded each other (Supplemental Table 1). In all remaining cases, random colocalizations were observed. Most of the tested proteins showed a large dynamic range where the number of positive colocalizations exceeded the other categories (Figure 8A). Interestingly, we found a minimum of one colocalization for all tested proteins except At4g00670 (Figures 8A and 8B; Supplemental Table 1). This Remorin protein labeled a unique microdomain population that is highly distinct from all other tested ones and showed colocalization only with itself. Similarly, the more evenly distributed At3g61260 did not colocalize with the majority of other domains (Figures 8A and 8B). In general, the number of significant R^2 values of colocalizing pairs greatly varied between the different proteins (Figure 8A). Proteins that are phylogenetically closely related (Raffaele et al., 2007) showed a tendency to increased colocalization (e.g., At2g41870/At3g57540 and At2g02170/At1g30320/At1g53860/At4g36970/At1g67590) (Figure 8B), implying that these microdomains may serve similar functions.

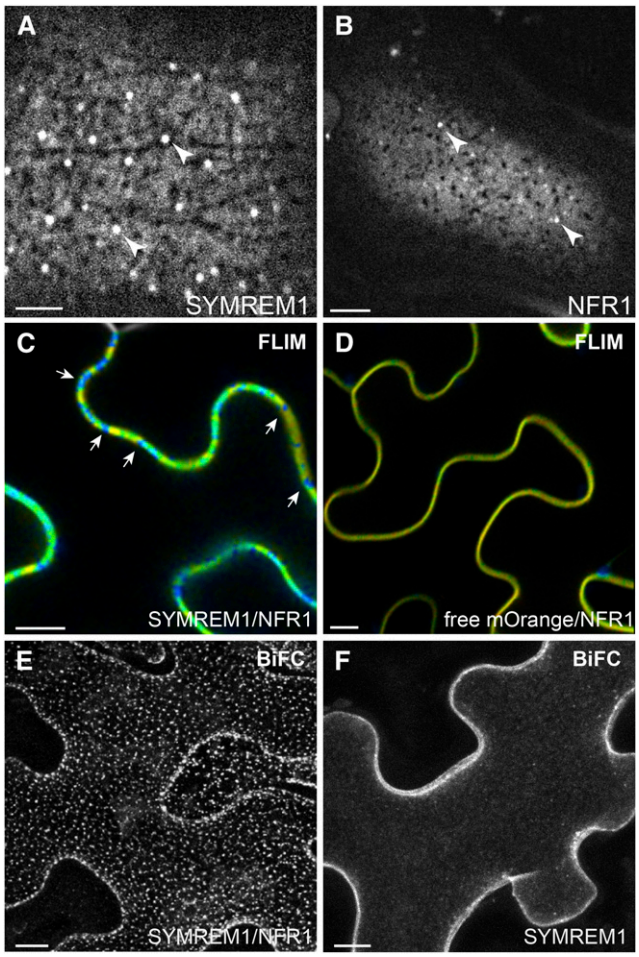

Figure 9. Membrane Domains May Provide Scaffolds for Protein–Protein Interactions.

(A) and **(B)** Heterologous expression of *L. japonicus* Remorin protein SYMREM1 **(A)** and NFR1 **(B)** in *N. benthamiana* leaf epidermal cells resulted in membrane domain labeling (arrowheads) at the cell surface. Bars = 5 μm.

(C) and **(D)** Donor fluorophore lifetime data obtained by fluorescence lifetime imaging microscopy (FLIM) and spectral photocounting on microscopic images. Cells expressing NFR1-Cerulean and SYMREM1-mOrange **(C)** and NFR1-Cerulean/free mOrange **(D)** showed interaction hotspots depicted in blue (decreased lifetime) **(C)** and homogenously distributed background signal **(D)** along the PM of *N. benthamiana* leaf epidermal cells. Bars = 10 μm.

(E) and **(F)** Compartmentalized interaction between SYMREM1 and NFR1 was also observed using bimolecular fluorescence complementation (BiFC) in *N. benthamiana* leaf epidermal cells. Less intense domains were found in BiFC assays testing homooligomerization of SMYREM1 **(F)**. Bars = 10 μm.

Perspectives: Protein–Protein Interactions Can Be Confined to Membrane Domains

Finally, we assessed whether receptor complex formation may be restricted to membrane domains. For this, we made use of an already described interaction between the Nod factor receptor NFR1 and the Remorin SYMREM1 from *Lotus japonicus* (Lefebvre et al., 2010; Tóth et al., 2012). Expression of fluorophore-tagged SYMREM1 (Figure 9A) and NFR1 (Figure 9B) in *N. benthamiana* leaf epidermal cells frequently resulted in clear labeling of distinct microdomains (arrowheads) as well as a more uniformly distributed protein fraction across the entire PM (Figures 9A and 9B), as described for other Remorin proteins (Figure 3). Using fluorescence lifetime imaging microscopy and Förster resonance energy transfer, we already demonstrated physical interactions between NFR1 and SYMREM1 (Tóth et al., 2012). To analyze the spatial patterning of protein interactions on the PM, the obtained photon counts were mapped onto cell images to investigate lateral variation in donor lifetimes across the PM. Interestingly, distinct sites of reduced fluorescence lifetime of the donor fluorophore (NFR1:Cerulean) were identified (blue), indicating interaction hotspots in membrane domains (Figure 9C). Similar patterns were observed for the interaction between the ATPase CDC48A and the receptor-like kinase SERK1 (Aker et al., 2007). No such foci were found in control experiments where we coexpressed NFR1 with the soluble acceptor fluorophore mOrange (Figure 9D). Similar results were obtained when performing bimolecular fluorescence complementation assays. Here, the NFR1 receptor and SYMREM1 were fused to the N-terminal and the C-terminal halves of the YFP fluorophore, respectively. Fluorescence was exclusively observed in distinct and immobile membrane domains that were distributed over the entire inner PM leaflet of transformed cells (Figure 9E). To exclude the possibility that the fluorescence was only due to protein accumulation in membrane domains, we studied SYMREM1 oligomerization. Here, no domain-restricted fluorescence was observed (Figure 9F), suggesting that Remorin–receptor interaction may indeed be delimited to membrane domains. Overall, these data indicate that laterally defined membrane domains may provide physical rafts for receptor–scaffold and other protein–protein interactions.

DISCUSSION

A number of cell biological studies revealed domain localization of PM-associated proteins such as Remorins (Raffaele et al., 2009; Lefebvre et al., 2010), Flotillins (Haney and Long, 2010; Li et al., 2012), the potassium channel KAT1 (Sutter et al., 2006; Reuff et al., 2010), the anion channel SLAC1 HOMOLOG3 (SLAH3) (Demir et al., 2013), the LysM receptor LYK3 (Haney et al., 2011), the NADPH oxidase RBOHD (Lherminier et al., 2009), and the exocyst protein SECA3 (Zhang et al., 2013). So far, all studies in plants were restricted to the analysis of individual proteins or a single protein pair. First insights into the coexistence of different membrane domains in plants were provided by the stimulus-dependent colocalization of FLOT4 and LYK3 (Haney et al., 2011). This observation is in agreement with the proposed function of Flotillins, which act as molecular scaffold proteins that mediate the assembly of domain platforms and can confer anchoring of membrane domains to the cytoskeleton (Langhorst et al., 2007). Similar functions have been proposed for Remorin proteins (Lefebvre et al., 2010; Tóth et al., 2012). Here, we took advantage of the genetic expansion of the Remorin gene family with 16 members in *Arabidopsis* to assess the diversity of microdomains that are targeted by members of

one specific family. Indeed, cloning and expression of almost all Remorin proteins revealed that the great majority of them predominantly localized to immobile microdomain platforms (Figures 2 and 3; Supplemental Figure 3). The existence of these domains was confirmed in different biological systems (Figures 2 and 3; Supplemental Figure 1). We found that members of the Remorin subgroup 1 (At3g61260, At2g45280, and At5g23750) (Raffaele et al., 2007) exhibited a more homogenous labeling of the PM surface. Interestingly, proteomic approaches identified only members of this subgroup in *Arabidopsis* DRMs (Shahollari et al., 2004; Kierszniowska et al., 2009; Minami et al., 2009; Keinath et al., 2010). In addition, closely related proteins showed either a similar pattern (At1g69325; group 3) or, in the cases of SYMREM1 (group 2) and At4g00670 (group 3), frequently labeled membrane domains, the latter at low density (Figure 3P). Together with the finding that group 1 Remorins may be targeted to distinct membrane domains in a stimulus- or tissue-dependent manner (Figure 6), these data indicate that evolutionarily related proteins target similar types of membrane domains. This hypothesis is supported by the fact that closely related proteins such as At3g57540 and At2g41870 (Figures 7I and 8B) or Remorins with extended N-terminal domains of group 6 (At2g02170, At1g30320, At1g53860, At4g36970, At1g67590, At1g13920, and At5g61280) generally displayed higher degrees of colocalization compared with phylogenetically distinct proteins (Figure 8). These data are also in line with a recent report regarding yeast, where extensive colocalization studies revealed that proteins with similar functions (e.g., hexose transporters) showed increased tendencies to colocalize in the same membrane compartment (Spira et al., 2012). Such functional specification of membrane domains would be biologically preferred not only to support protein complex formation but also to physically separate enzymatic activities of physiologically unrelated processes. This hypothesis is supported by a recent study that demonstrated a colocalization of the *Arabidopsis* anion channel SLAH3 with the calcium-dependent protein kinase CPK21 in membrane microdomains. Interestingly, coexpression of the SLAH3/CPK21 complex with the PROTEIN PHOSPHATASE 2C (PP2C) phosphatase ABI1 led to a displacement from microdomains. This correlated with a loss of SLAH3 functionality (Demir et al., 2013). Similarly, mistargeting of the FERRO-O2-OXIDOREDUCTASE Fet3 to the membrane domain labeled by PLASMA MEMBRANE PROTEIN1 (Pmp1) by transmembrane domain replacement resulted in impaired iron uptake in yeast even though full enzymatic activity of the Fet3-Pmp1 chimera needs to be demonstrated (Spira et al., 2012). For Remorin proteins that were analyzed in this study, these data imply that even though they may serve similar molecular functions, different members could be involved in distinct biological processes.

Almost all membrane domains investigated in this study formed structures that were immobile (Figures 4 and 5D). These domains are predominantly maintained by lateral protein diffusion, indicated by rather slow and centripetal fluorescence recovery (Figure 5), which has been reported for other PM-associated proteins before (Bhat et al., 2005; Martinière et al., 2012; Spira et al., 2012). Interestingly, no differences in recovery half-times and mobile fractions were observed between a membrane domain–associated fraction and a freely membrane-bound fraction (Figures 5B and 5C). Two physical scaffolds may mediate such stability: the cell wall and the cortical cytoskeleton. Using protoplasts that continuously rebuild a cell wall after its enzymatic removal, a recent study showed that the lateral mobility of proteins was significantly altered during cell wall regeneration (Martinière et al., 2012). In addition, cortical actin and microtubule arrays can serve as fences or anchoring scaffolds for membrane domains (reviewed in Kusumi et al., 2005, 2012). In line with data from yeast, where microtubules stabilized membrane domains (Spira et al., 2012), at least a fraction of At1g13920 that targets a filament-like structure in the PM was also found to be sensitive to oryzalin treatment (Supplemental Figure 5D). However, while the role of actin in membrane domain stabilization remains to be demonstrated in plants, recent data from human cells suggest active roles of this cytoskeleton component in the lateral immobilization of membrane compartments (Dinic et al., 2013). Such dependence on the cytoskeleton may also explain why processes like the invasion of host cells by pathogenic fungi that are accompanied by cortical rearrangement (Henty-Ridilla et al., 2013) trigger the accumulation of sterol-rich membrane domains and resistance proteins at the site of cell penetration (Bhat et al., 2005; Underwood and Somerville, 2013). Therefore, it will be a future challenge to dissect the functional specification and diversity of membrane domains during plant–microbe interactions. Remorin- and Flotillin-labeled microdomains are likely to harbor unique sets of signaling proteins or to serve as signaling platforms (Figure 9) required for plant cell responses toward pathogenic and symbiotic microbes (Jarsch and Ott, 2011; Urbanus and Ott, 2012). Thus, the identification of the microdomain proteome will allow detailed understanding of supercomplexes and potential modes of regulation.

METHODS

Cloning and Constructs

For ectopic expression, 10 of the 16 *Arabidopsis thaliana* Remorins were obtained as cDNA clones from RIKEN (http://www.brc.riken.jp/lab/epd/catalog/cdnaclone.html). At5g23750, At1g69325, At1g67590, and At5g61280 were amplified from *Arabidopsis* cDNA generated by reverse transcription of RNA from *Nicotiana benthamiana* plants overexpressing the respective genomic constructs. At1g13920 was amplified from *Arabidopsis* genomic DNA. We created Gateway (GW)-compatible entry vectors for N-terminal fluorophore fusions. As destination vectors for ectopic overexpression, we used pAM-PAT-35SS:YFP:GW, pAM-PAT-35SS:CFP:GW, and pUBI-YFP:GW, respectively (Maekawa et al., 2008; Tóth et al., 2012). For the expression of N-terminally tagged fluorophore fusions under the control of the endogenous promoter, we created subclones of the putative 2-kb promoter region, the fluorophore, and the genomic coding sequence. Those fragments joined with *Bsa*I recognition sites and individual overhangs were blunt-end ligated into a modified puc57 and subsequently assembled via cut ligation into a modified pENTR-D. Expression vectors were created with pGWB1 (Binder et al., 2014). All primers used in this study are listed in Supplemental Table 2.

Plant Material and Quantitative Real-Time PCR

For stable transformations of N-terminally tagged Remorin constructs under the control of their respective endogenous promoters, the

following *Arabidopsis* T-DNA insertion lines were obtained: At3g61260 (SALK_117637.50.50.x), At2g45820 (SALK_17448.53.95.x), and At4g36970 (SALK_037050.55.00.x). For transient transformations of *Arabidopsis*, transgenic lines expressing a *ProDEX:AvrPto* construct (Hauck et al., 2003; Tsuda et al., 2012) were used. Transcript levels in the *at4g36970-1* mutant were determined by quantitative real-time PCR on cDNA of three independent biological replicates obtained from young rosette leaves of plants grown in a greenhouse using a SYBR Green assay. Data were normalized to the expression of PP2A as described elsewhere (Czechowski et al., 2005). Protein gel blot analysis was performed on plant material grown under the same conditions using the α-REM antibody at a 1:3000 dilution as described earlier (Raffaele et al., 2009).

Protein Expression for Fluorescence Microscopy

Agrobacterium tumefaciens–mediated transient transformation of *N. benthamiana* was performed as described earlier (Tóth et al., 2012). For single infiltrations, pAM-PAT 35S constructs were used. To avoid promoter silencing during coexpression, we used one construct driven by the 35S promoter and one driven by the pUbiquitin (pUbi) promoter. For infiltration of pUbi-driven constructs, we used final OD_{600} values of 0.01 and 0.005; for pAM-PAT-35S, we used final OD_{600} values of 0.2 to 0.4 for colocalization experiments and 0.01 for the expression of single proteins. *Agrobacterium*-mediated transient transformation of *Arabidopsis* was performed in stable lines carrying a *ProDEX:AvrPto* construct (Tsuda et al. 2012). For dexamethasone pretreatment, plants were sprayed with a 2 μM dexamethasone solution containing 0.04% Silwett-77 24 h prior to transformation. Microscopical analysis was performed 2 d after infiltration as described below.

Plant Growth and Stable Transformation

N. benthamiana plants were grown 4 to 5 weeks under greenhouse conditions. *ProDEX:AvrPto Arabidopsis* plants were grown 5 to 6 weeks under short-day conditions (16 h of dark, 18°C/8 h of light, 20°C). *Arabidopsis* lines for stable transformation were grown 4 weeks under long-day conditions (8 h of dark/16 h of light) in the greenhouse. Shoots were cut back and plants regrown for 1 more week prior to floral dipping (Clough and Bent, 1998). Selection of stable transformants on hygromycin-containing plates was performed according to Harrison et al. (2006).

Confocal Microscopy and Quantitative Image Analysis

Standard confocal microscopy was performed with a Leica TCS SP5 confocal laser scanning microscope using an argon laser. YFP and CFP fluorophores were excited with the 514- and 456-nm laser lines, and emission was recorded in the range of 525 to 600 nm and 475 to 520 nm, respectively. Images were taken with a Leica DFC350FX digital camera.

For quantitative image analysis of individually expressed proteins, 10 images were segmented to differentiate between background and domains using a threshold of 0, 15 to 0, 22 and a background subtraction with a rolling ball radius of 20 pixels. The Fiji plugin Watershed was applied to separate overlapping intensities. The resulting image was used as a mask for an overlay on the original image. All quantitative measurements were then performed on the unprocessed image. Average values for domain size, mean domain intensity, circularity, and density were depicted as box plots using R. Statistical analysis was performed in R using ANOVA and Tukey's honestly significant difference.

For colocalization analysis, single images were subjected to a mean blur of 2 pixels and a background subtraction with a rolling ball radius of 20 pixels. Intensity correlation analysis using the respective plugin for ImageJ provided by the Wright Cell Imaging Facility (Li et al., 2004) was performed to calculate both the Pearson correlation coefficient (Manders et al., 1992) and the R^2 (Manders et al., 1993). Mean values of an average of 12 repetitions were calculated. Simulations for random distribution patterns of each investigated protein pair were performed on reflected or rotated images, selecting ROIs containing relevant signal information in both channels. Between 8 and 17 values of colocalizing and randomized samples of one protein pair were used for a Student's *t* test to determine the significance of positive or negative correlations.

FRAP analysis was performed using FRAP Wizard implemented in the Leica LAS AF software. One frame was scanned prior to bleaching. Bleaching was performed on a circular ROI of 5 μm in diameter in 10 frames with 100% laser intensity (~15 s). For single-domain bleaching (Figures 5D and 5E), this ROI was decreased to 2 μm. Fluorescence recovery was imaged in 30-s intervals over 10 frames. FRAP values were fitted as described previously (Spira et al., 2012) using a simple exponential fit of $y = a \times (1.0 - \exp(bx))$. Half times [$t_{1/2} = \ln(0.5)/b$] and mobile fractions [$Mf = (a \times 100)/\text{linorm}$] were calculated for all FRAP experiments with a fit higher than 0.97. Surface plots were calculated from single ROIs in ImageJ.

For kymographs, films were acquired over a time frame of at least 20 min. Z-stacks with 15 to 18 slices of 1 μm thickness were recorded every 2 min. Single images from Z-stacks of each time point were combined into stacks and transformed into Z-projects with maximal intensities in Fiji. All 10 Z-project images were again combined into a stack and corrected for eventual lateral shift of the sample via the Fiji plugin StackReg (Rigid Body). A line of 20 μm was drawn, and the kymograph was created via the Reslice [/] tool of Fiji.

The colocalization network was visualized using Cytoscape software (Shannon et al., 2003). Layout of the network was done manually. As indicated in the figure legends, the line width indicates the probability of the observed correlation occurring by random (gray) and the color indicates whether the two proteins colocalized (blue) or were found in mutually exclusive localizations (red).

TIRFM

TIRFM was performed on leaves of 2-week-old seedlings grown sterile on plates. Images were acquired on an iMIC stand (Till Photonics) with an Olympus 100× 1.45 numerical aperture objective. A diode-pumped solid state laser (75 mW) at 488 nm (Coherent Sapphire) was selected through an accusto-optical tunable filter. A two-axis scan head was used to adjust incidence angles. Images were collected with an Andor iXON DU-897 EMCCD camera controlled by Live Acquisition (Till Photonics) software.

Drug Treatments

A 1 mM stock solution of oryzalin was prepared using DMSO as solvent and diluted to a final concentration of 5 μM. Leaf discs were incubated for 4 h before imaging. For latrunculin B, a 2.4 μM stock solution in ethanol was diluted in water to a final concentration of 50 nM. Leaf discs were incubated in the latrunculin B solution for 3 h before imaging. All controls were incubated in the respective solvent that was diluted accordingly.

Accession Numbers

Sequence data from this article can be found in the GenBank/EMBL data libraries under the following accession numbers: FLOT1A (At5g25250), FLOT1B (At5g25260), KAT1 (At5g46240), potato REM1.3 (NM_001288060), and SYMREM1 (JQ061257). Gene expression data (Figure 1A) are available in the Genevestigator database (repository identifiers GSM768250, GSM768251, and GSM768252) with the following accession numbers: *at3g61260-1* (SALK_117639), *at3g61260-2* (SALK_117637), *at2g45820-1* (SALK_011986), *at2g45820-2* (SALK_17448), and *at4g36970-1* (SALK_037050).

Supplemental Data

The following materials are available in the online version of this article.

Supplemental Figure 1. Membrane Domain Localization of Different Remorin Proteins in *Arabidopsis* and *N. benthamiana*.

Supplemental Figure 2. Total Internal Reflection Microscopy (TIRFM) of Upper Plasma Membrane Planes.

Supplemental Figure 3. Confocal Images of Secant Planes Illustrate the Plasma Membrane Localization of All 18 Marker Proteins.

Supplemental Figure 4. Quantification of Membrane Domain Parameters of All Marker Proteins.

Supplemental Figure 5. Filament-Like Localization of At1g13290 Is Dependent on Microtubules.

Supplemental Figure 6. Image Processing and Randomization for Quantitative Analysis of Colocalizations.

Supplemental Table 1. Data from Quantitative Image Analysis of Colocalization Experiments.

Supplemental Table 2. List of Primers Used in This Study.

ACKNOWLEDGMENTS

We thank members of our laboratory for fruitful discussions. We thank Macarena Marín and Claudia Popp for critical reading of the article, Guido Grossmann (Centre for Organismal Studies, Heidelberg, Germany) and Simon Brandner for valuable advice on image analysis, and Martina Ried for help with R. We also thank Jessica Folgmann for excellent technical assistance and Roland Wedlich-Söldner (Max-Planck-Institute for Biochemistry) for access to the total internal reflection microscope. The potato REM1.3 clone and the α-REM antibody were kind gifts from Sylvain Raffaele (Laboratoire des Interactions Plantes-Microorganismes, Toulouse, France) and Sebastien Mongrand (University of Bordeaux). The LifeAct template was provided by the laboratory of Stefanie Sprunck (University of Regensburg). This work was supported by the Deutsche Forschungsgemeinschaft from the Emmy-Noether Programme (Grant OT423/2-1) and the Collaborative Research Center 924 (Grant Sonderforschungsbereich 924), by the University of Bavaria (Ph.D. fellowships to I.K.J. and S.S.A.K.), and the Boehringer Ingelheim Foundation.

AUTHOR CONTRIBUTIONS

I.K.J., S.S.A.K., and T.O. designed the research. I.K.J., S.S.A.K., T.F.S., S.L.U., K.-H.B., W.S., and T.O. performed research. I.K.J., S.S.A.K., T.F.S., P.B., and T.O. analyzed data. I.K.J. and T.O. wrote the article.

Received February 18, 2014; revised March 17, 2014; accepted March 24, 2014; published April 8, 2014.

REFERENCES

Aker, J., Hesselink, R., Engel, R., Karlova, R., Borst, J.W., Visser, A.J., and de Vries, S.C. (2007). In vivo hexamerization and characterization of the Arabidopsis AAA ATPase CDC48A complex using Forster resonance energy transfer-fluorescence lifetime imaging microscopy and fluorescence correlation spectroscopy. Plant Physiol. **145:** 339–350.

Bhat, R.A., Miklis, M., Schmelzer, E., Schulze-Lefert, P., and Panstruga, R. (2005). Recruitment and interaction dynamics of plant penetration resistance components in a plasma membrane microdomain. Proc. Natl. Acad. Sci. USA **102:** 3135–3140.

Binder, A., Lambert, J., Morbitzer, R., Popp, C., Ott, T., Lahaye, T., and Parniske, M. (2014). A modular plasmid assembly kit for multigene expression, gene silencing and silencing rescue in plants. PLoS ONE **9:** e88218.

Boutté, Y., and Grebe, M. (2009). Cellular processes relying on sterol function in plants. Curr. Opin. Plant Biol. **12:** 705–713.

Clough, S.J., and Bent, A.F. (1998). Floral dip: A simplified method for *Agrobacterium*-mediated transformation of *Arabidopsis thaliana*. Plant J. **16:** 735–743.

Czechowski, T., Stitt, M., Altmann, T., Udvardi, M.K., and Scheible, W.R. (2005). Genome-wide identification and testing of superior reference genes for transcript normalization in Arabidopsis. Plant Physiol. **139:** 5–17.

Demir, F., Horntrich, C., Blachutzik, J.O., Scherzer, S., Reinders, Y., Kierszniowska, S., Schulze, W.X., Harms, G.S., Hedrich, R., Geiger, D., and Kreuzer, I. (2013). Arabidopsis nanodomain-delimited ABA signaling pathway regulates the anion channel SLAH3. Proc. Natl. Acad. Sci. USA **110:** 8296–8301.

Dinic, J., Ashrafzadeh, P., and Parmryd, I. (2013). Actin filaments attachment at the plasma membrane in live cells cause the formation of ordered lipid domains. Biochim. Biophys. Acta **1828:** 1102–1111.

Haney, C.H., and Long, S.R. (2010). Plant flotillins are required for infection by nitrogen-fixing bacteria. Proc. Natl. Acad. Sci. USA **107:** 478–483.

Haney, C.H., Riely, B.K., Tricoli, D.M., Cook, D.R., Ehrhardt, D.W., and Long, S.R. (2011). Symbiotic rhizobia bacteria trigger a change in localization and dynamics of the *Medicago truncatula* receptor kinase LYK3. Plant Cell **23:** 2774–2787.

Harrison, S.J., Mott, E.K., Parsley, K., Aspinall, S., Gray, J.C., and Cottage, A. (2006). A rapid and robust method of identifying transformed *Arabidopsis thaliana* seedlings following floral dip transformation. Plant Methods **2:** 19.

Hauck, P., Thilmony, R., and He, S.Y. (2003). A *Pseudomonas syringae* type III effector suppresses cell wall-based extracellular defense in susceptible Arabidopsis plants. Proc. Natl. Acad. Sci. USA **100:** 8577–8582.

Henty-Ridilla, J.L., Shimono, M., Li, J., Chang, J.H., Day, B., and Staiger, C.J. (2013). The plant actin cytoskeleton responds to signals from microbe-associated molecular patterns. PLoS Pathog. **9:** e1003290.

Jarsch, I.K., and Ott, T. (2011). Perspectives on remorin proteins, membrane rafts, and their role during plant-microbe interactions. Mol. Plant Microbe Interact. **24:** 7–12.

Keinath, N.F., Kierszniowska, S., Lorek, J., Bourdais, G., Kessler, S.A., Shimosato-Asano, H., Grossniklaus, U., Schulze, W.X., Robatzek, S., and Panstruga, R. (2010). PAMP (pathogen-associated molecular pattern)-induced changes in plasma membrane compartmentalization reveal novel components of plant immunity. J. Biol. Chem. **285:** 39140–39149.

Kierszniowska, S., Seiwert, B., and Schulze, W.X. (2009). Definition of Arabidopsis sterol-rich membrane microdomains by differential treatment with methyl-beta-cyclodextrin and quantitative proteomics. Mol. Cell. Proteomics **8:** 612–623.

Kusumi, A., Fujiwara, T.K., Chadda, R., Xie, M., Tsunoyama, T.A., Kalay, Z., Kasai, R.S., and Suzuki, K.G. (2012). Dynamic organizing principles of the plasma membrane that regulate signal transduction: Commemorating the fortieth anniversary of Singer and Nicolson's fluid-mosaic model. Annu. Rev. Cell Dev. Biol. **28:** 215–250.

Kusumi, A., Nakada, C., Ritchie, K., Murase, K., Suzuki, K., Murakoshi, H., Kasai, R.S., Kondo, J., and Fujiwara, T. (2005). Paradigm shift of the plasma membrane concept from the two-dimensional continuum fluid to the partitioned fluid: High-speed single-molecule tracking of membrane molecules. Annu. Rev. Biophys. Biomol. Struct. **34:** 351–378.

Langhorst, M.F., Solis, G.P., Hannbeck, S., Plattner, H., and Stuermer, C.A. (2007). Linking membrane microdomains to the cytoskeleton: Regulation of the lateral mobility of reggie-1/flotillin-2 by interaction with actin. FEBS Lett. **581:** 4697–4703.

Lefebvre, B., et al. (2010). A remorin protein interacts with symbiotic receptors and regulates bacterial infection. Proc. Natl. Acad. Sci. USA **107:** 2343–2348.

Levental, I., Grzybek, M., and Simons, K. (2010a). Greasing their way: Lipid modifications determine protein association with membrane rafts. Biochemistry **49:** 6305–6316.

Levental, I., Lingwood, D., Grzybek, M., Coskun, U., and Simons, K. (2010b). Palmitoylation regulates raft affinity for the majority of integral raft proteins. Proc. Natl. Acad. Sci. USA **107:** 22050–22054.

Lherminier, J., Elmayan, T., Fromentin, J., Elaraqui, K.T., Vesa, S., Morel, J., Verrier, J.L., Cailleteau, B., Blein, J.P., and Simon-Plas, F. (2009). NADPH oxidase-mediated reactive oxygen species production: Subcellular localization and reassessment of its role in plant defense. Mol. Plant Microbe Interact. **22:** 868–881.

Li, Q., Lau, A., Morris, T.J., Guo, L., Fordyce, C.B., and Stanley, E.F. (2004). A syntaxin 1, Galpha(o), and N-type calcium channel complex at a presynaptic nerve terminal: Analysis by quantitative immunocolocalization. J. Neurosci. **24:** 4070–4081.

Li, R., Liu, P., Wan, Y., Chen, T., Wang, Q., Mettbach, U., Baluska, F., Samaj, J., Fang, X., Lucas, W.J., and Lin, J. (2012). A membrane microdomain-associated protein, *Arabidopsis* Flot1, is involved in a clathrin-independent endocytic pathway and is required for seedling development. Plant Cell **24:** 2105–2122.

Lingwood, D., and Simons, K. (2010). Lipid rafts as a membrane-organizing principle. Science **327:** 46–50.

Maekawa, T., Kusakabe, M., Shimoda, Y., Sato, S., Tabata, S., Murooka, Y., and Hayashi, M. (2008). Polyubiquitin promoter-based binary vectors for overexpression and gene silencing in *Lotus japonicus*. Mol. Plant Microbe Interact. **21:** 375–382.

Malinsky, J., Opekarová, M., Grossmann, G., and Tanner, W. (2013). Membrane microdomains, rafts, and detergent-resistant membranes in plants and fungi. Annu. Rev. Plant Biol. **64:** 501–529.

Malinsky, J., Opekarová, M., and Tanner, W. (2010). The lateral compartmentation of the yeast plasma membrane. Yeast **27:** 473–478.

Manders, E.M., Stap, J., Brakenhoff, G.J., van Driel, R., and Aten, J.A. (1992). Dynamics of three-dimensional replication patterns during the S-phase, analysed by double labelling of DNA and confocal microscopy. J. Cell Sci. **103:** 857–862.

Manders, E.M., Verbeek, F.J., and Aten, J.A. (1993). Measurement of co-localization of objects in dual-colour confocal images. J. Microsc. **169:** 375–382.

Marín, M., and Ott, T. (2012). Phosphorylation of intrinsically disordered regions in remorin proteins. Front. Plant Sci. **3:** 86.

Marín, M., Thallmair, V., and Ott, T. (2012). The intrinsically disordered N-terminal region of AtREM1.3 remorin protein mediates protein-protein interactions. J. Biol. Chem. **287:** 39982–39991.

Martinière, A., et al. (2012). Cell wall constrains lateral diffusion of plant plasma-membrane proteins. Proc. Natl. Acad. Sci. USA **109:** 12805–12810.

Minami, A., Fujiwara, M., Furuto, A., Fukao, Y., Yamashita, T., Kamo, M., Kawamura, Y., and Uemura, M. (2009). Alterations in detergent-resistant plasma membrane microdomains in *Arabidopsis thaliana* during cold acclimation. Plant Cell Physiol. **50:** 341–359.

Müller, A., Guan, C., Gälweiler, L., Tänzler, P., Huijser, P., Marchant, A., Parry, G., Bennett, M., Wisman, E., and Palme, K. (1998). AtPIN2 defines a locus of Arabidopsis for root gravitropism control. EMBO J. **17:** 6903–6911.

Raffaele, S., et al. (2009). Remorin, a Solanaceae protein resident in membrane rafts and plasmodesmata, impairs potato virus X movement. Plant Cell **21:** 1541–1555.

Raffaele, S., Mongrand, S., Gamas, P., Niebel, A., and Ott, T. (2007). Genome-wide annotation of remorins, a plant-specific protein family: Evolutionary and functional perspectives. Plant Physiol. **145:** 593–600.

Reuff, M., Mikosch, M., and Homann, U. (2010). Trafficking, lateral mobility and segregation of the plant K channel KAT1. Plant Biol. (Stuttg.) **12** (suppl. 1)**:** 99–104.

Roppolo, D., De Rybel, B., Tendon, V.D., Pfister, A., Alassimone, J., Vermeer, J.E., Yamazaki, M., Stierhof, Y.D., Beeckman, T., and Geldner, N. (2011). A novel protein family mediates Casparian strip formation in the endodermis. Nature **473:** 380–383.

Russinova, E., Borst, J.W., Kwaaitaal, M., Caño-Delgado, A., Yin, Y., Chory, J., and de Vries, S.C. (2004). Heterodimerization and endocytosis of *Arabidopsis* brassinosteroid receptors BRI1 and AtSERK3 (BAK1). Plant Cell **16:** 3216–3229.

Shahollari, B., Peskan-Berghoefer, T., and Oelmueller, R. (2004). Receptor kinases with leucine-rich repeats are enriched in Triton X-100 insoluble plasma membrane microdomains from plants. Physiol. Plant. **122:** 397–403.

Shannon, P., Markiel, A., Ozier, O., Baliga, N.S., Wang, J.T., Ramage, D., Amin, N., Schwikowski, B., and Ideker, T. (2003). Cytoscape: A software environment for integrated models of biomolecular interaction networks. Genome Res. **13:** 2498–2504.

Spira, F., Mueller, N.S., Beck, G., von Olshausen, P., Beig, J., and Wedlich-Söldner, R. (2012). Patchwork organization of the yeast plasma membrane into numerous coexisting domains. Nat. Cell Biol. **14:** 640–648.

Sutter, J.U., Campanoni, P., Tyrrell, M., and Blatt, M.R. (2006). Selective mobility and sensitivity to SNAREs is exhibited by the *Arabidopsis* KAT1 K^+ channel at the plasma membrane. Plant Cell **18:** 935–954.

Tanner, W., Malinsky, J., and Opekarová, M. (2011). In plant and animal cells, detergent-resistant membranes do not define functional membrane rafts. Plant Cell **23:** 1191–1193.

Tóth, K., Stratil, T.F., Madsen, E.B., Ye, J., Popp, C., Antolín-Llovera, M., Grossmann, C., Jensen, O.N., Schüssler, A., Parniske, M., and Ott, T. (2012). Functional domain analysis of the Remorin protein LjSYMREM1 in *Lotus japonicus*. PLoS ONE **7:** e30817.

Tsuda, K., Qi, Y., Nguyen, V., Bethke, G., Tsuda, Y., Glazebrook, J., and Katagiri, F. (2012). An efficient Agrobacterium-mediated transient transformation of Arabidopsis. Plant J. **69:** 713–719.

Underwood, W., and Somerville, S.C. (2013). Perception of conserved pathogen elicitors at the plasma membrane leads to relocalization of the Arabidopsis PEN3 transporter. Proc. Natl. Acad. Sci. USA **110:** 12492–12497.

Urbanus, S.L., and Ott, T. (2012). Plasticity of plasma membrane compartmentalization during plant immune responses. Front. Plant Sci. **3:** 181.

van den Bogaart, G., Meyenberg, K., Risselada, H.J., Amin, H., Willig, K.I., Hubrich, B.E., Dier, M., Hell, S.W., Grubmüller, H., Diederichsen, U., and Jahn, R. (2011). Membrane protein sequestering by ionic protein-lipid interactions. Nature **479:** 552–555.

Vermeer, J.E., Van Munster, E.B., Vischer, N.O., and Gadella, T.W., Jr.,. (2004). Probing plasma membrane microdomains in cowpea protoplasts using lipidated GFP-fusion proteins and multimode FRET microscopy. J. Microsc. **214:** 190–200.

Zhang, Y., Immink, R., Liu, C.M., Emons, A.M., and Ketelaar, T. (2013). The Arabidopsis exocyst subunit SEC3A is essential for embryo development and accumulates in transient puncta at the plasma membrane. New Phytol. **199:** 74–88.

Zurzolo, C., van Meer, G., and Mayor, S. (2003). The order of rafts. Conference on microdomains, lipid rafts and caveolae. EMBO Rep. **4:** 1117–1121.